

# Inverse Problems and Imaging

## Presentation - Project Assignment

Adonis JAMAL   Jean-Vincent MARTINI  
Reverse-time and Kirchhoff migration

Ecole Normale Supérieure Paris-Saclay  
MVA 2025-2026

March 27th, 2026

école  
normale  
supérieure  
paris-saclay



# Overview and Objectives

**Goal:** Reconstruct the location of a point-like reflector from time-harmonic or broadband measurement data in 2D, using synthetic array data.

## Configurations studied:

- **Full aperture:** circular array of  $N$  transducers
- **Partial aperture:** linear array along the  $x$ -axis
- **Time-dependent:** broadband signal emission
- **Noisy setting:** additive complex Gaussian noise

## Methods compared:

Reverse-Time (RT) migration,  
Kirchhoff Migration (KM),  
MUSIC-type.

## Workflow:

- ① Derive the Green's function and generate synthetic data via Born approximation
- ② Define and implement RT, KM, MUSIC functionals
- ③ Analyze results
- ④ Study stability under noise (Monte Carlo)

# Green's Function and Data Model

**Green's function.** We assume propagation speed  $c_0 = 1$ . The 2D homogeneous Green's function  $\hat{G}_0(\omega, x, y)$  satisfies:

$$\Delta_x \hat{G}_0 + \omega^2 \hat{G}_0 = -\delta(x - y), \quad x \in \mathbb{R}^2$$

with the Sommerfeld radiation condition. It is given explicitly by:

$$\hat{G}_0(\omega, x, y) = \frac{i}{4} H_0^{(1)}(\omega|x - y|)$$

where  $H_0^{(1)}(s) = J_0(s) + iY_0(s)$  is the Hankel function of the first kind.

**Data model (Born approximation).** For a point-like reflector at  $\mathbf{x}_{\text{ref}}$ , the data matrix entry for receiver  $r$  and source  $s$  is:

$$\hat{u}_{rs}(\omega) = \omega^2 \hat{G}_0(\omega, \mathbf{x}_r, \mathbf{x}_{\text{ref}}) \hat{G}_0(\omega, \mathbf{x}_{\text{ref}}, \mathbf{x}_s)$$

which can be written in matrix form as:

$$\hat{U}(\omega) = -\frac{\omega^2}{16} \mathbf{v} \mathbf{v}^T, \quad v_t = H_0^{(1)}(\omega|\mathbf{x}_t - \mathbf{x}_{\text{ref}}|)$$

# RT, KM and MUSIC Imaging Functionals

**Reverse-Time (RT) migration:**

$$\mathcal{I}_{RT}(\mathbf{x}) = \frac{1}{2\pi} \int_{-\infty}^{\infty} d\omega \sum_{r,s} \overline{\hat{G}_0(\omega, \mathbf{x}, \mathbf{x}_r)} \hat{u}_{rs}(\omega) \overline{\hat{G}_0(\omega, \mathbf{x}_s, \mathbf{x})}$$

**Kirchhoff Migration (KM):** from RT, with  $\hat{G}_0(\omega, \mathbf{x}, \mathbf{y}) \approx e^{i\omega T(\mathbf{x}, \mathbf{y})}$ :

$$\mathcal{I}_{KM}(\mathbf{x}) = \frac{1}{2\pi} \int_{-\infty}^{\infty} d\omega \sum_{r,s} e^{-i\omega|\mathbf{x}-\mathbf{x}_r|} \hat{u}_{rs}(\omega) e^{-i\omega|\mathbf{x}_s-\mathbf{x}|}$$

**MUSIC** (partial aperture, noise-subspace variant):

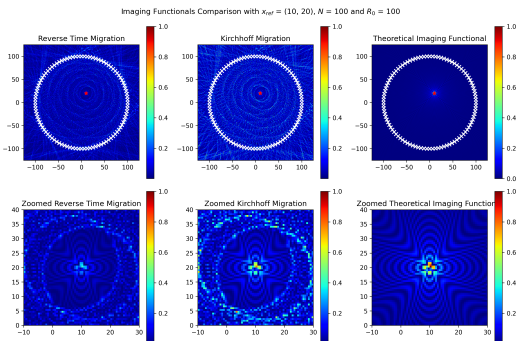
$$\mathcal{I}_{MU}(\mathbf{x}) = \frac{1}{1 - |\langle \hat{g}(\omega, \mathbf{x}), v_1 \rangle|^2}$$

where  $\hat{g}(\omega, \mathbf{x}) = (\hat{G}_0(\omega, \mathbf{x}, \mathbf{x}_r))_{r=1,\dots,N}$  and  $v_1$  is the first singular vector of  $\hat{U}$ .

**Theoretical focal spots:** Full aperture  $\sim J_0^2(\omega|x - x_{ref}|)$ ; Partial aperture: sinc<sup>2</sup> in cross-range, Fresnel integral in range.

# Full Aperture – RT, KM and Theoretical Focal Spot

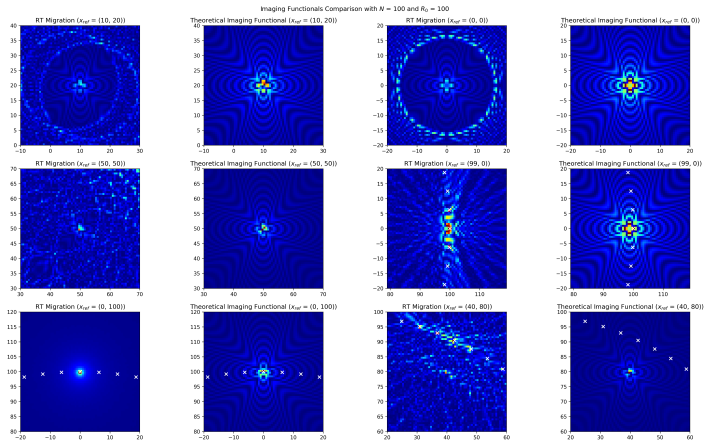
**Setup:**  $N = 100$  transducers on a circle,  $R_0 = 100$ ,  $\omega = 2\pi$ ,  
 $x_{\text{ref}} = (10, 20)$ .



- RT and KM images are very similar; minor discrepancies come from the approximation used in KM.
- The theoretical  $J_0^2$  focal spot differs noticeably: it is derived under the asymptotic limit  $R_0 \rightarrow \infty$ ,  $N \rightarrow \infty$ .
- Near the reflector, all three profiles agree qualitatively.

# Full Aperture – Multiple Reflector Positions

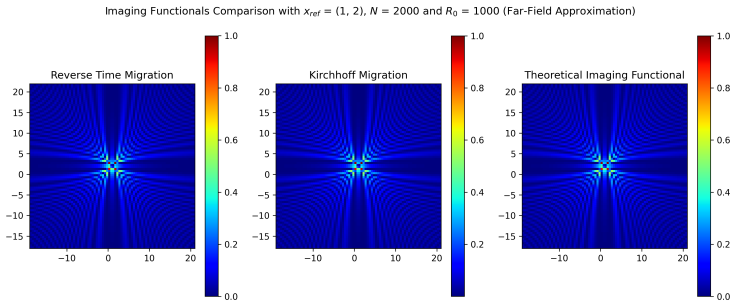
**Effect of reflector position:** reflector moved to  $(0, 0)$ ,  $(0, 100)$ ,  $(100, 0)$ .



As the reflector approaches the array boundary, the asymptotic assumptions break down and the discrepancy between RT/KM and the theoretical  $J_0^2$  profile becomes more pronounced.

# Full Aperture – Far-Field Regime

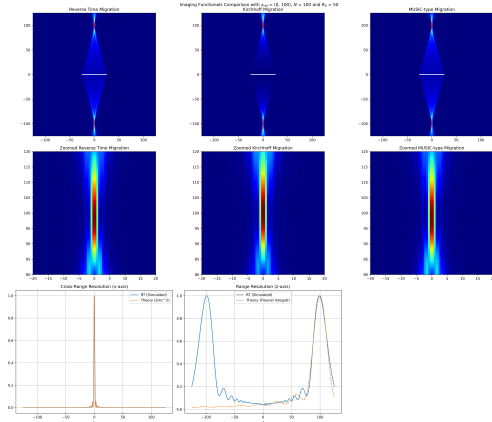
**Far-field regime:**  $R_0 = 1000$ ,  $N = 2000$ .



With a much larger array and many more transducers, the RT and KM functionals converge closely to the theoretical  $J_0^2$  focal spot, confirming the validity of the asymptotic formula in the appropriate regime.

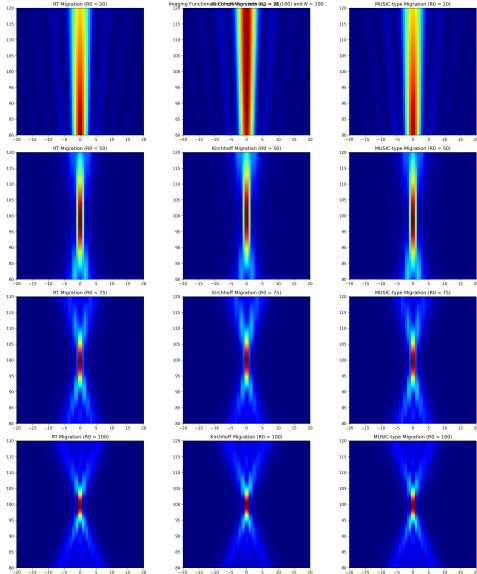
# Partial Aperture – RT, KM and MUSIC

**Setup:**  $N = 100$  transducers on a linear array,  $R_0 = 100$ ,  $\omega = 2\pi$ ,  $\mathbf{x}_{\text{ref}} = (10, 20)$ .



- RT, KM and MUSIC closely resemble each other.
- **Cross-range ( $x$ ):** RT reproduces the main peak and secondary lobes almost perfectly.
- **Range ( $z$ ):** a mirror image appears at  $-z_{\text{ref}}$  due to the linear geometry (transducers on the  $x$ -axis cannot distinguish  $z$  from  $-z$ ).

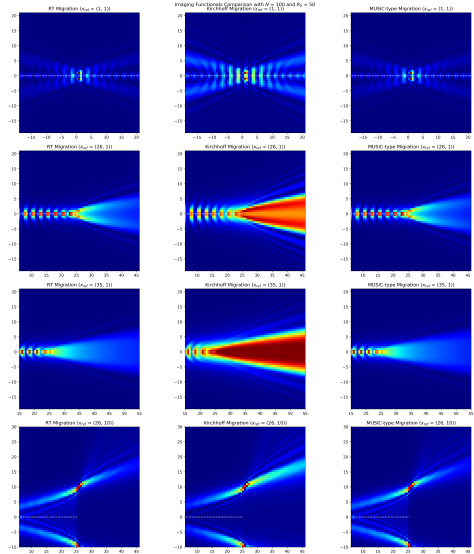
# Partial Aperture – Influence of Array Length $R_0$



**Varying  $R_0$ :** smaller aperture  
⇒ coarser cross-range  
resolution (larger  
 $r_c = \lambda|x_{\text{ref}}|/R_0$ ).

As  $R_0$  decreases, the focal spot widens in the cross-range direction, consistent with the theoretical  $\text{sinc}^2$  prediction.

# Partial Aperture – Multiple Reflector Positions

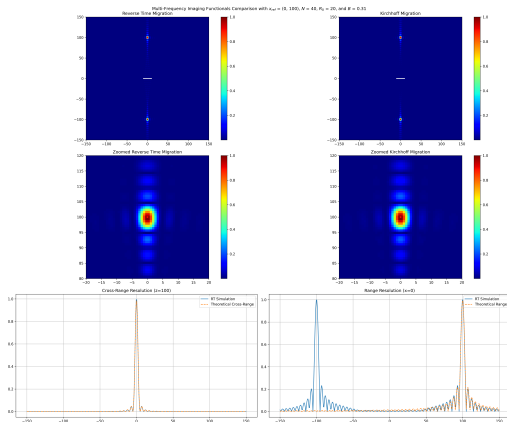


**Varying  $x_{\text{ref}}$ :** moving the reflector further from the array increases the range and degrades cross-range resolution.

The focal spot characteristics scale with the stand-off distance  $|x_{\text{ref}}|$ , in agreement with the theoretical expressions for  $r_c$  and  $r_f$ .

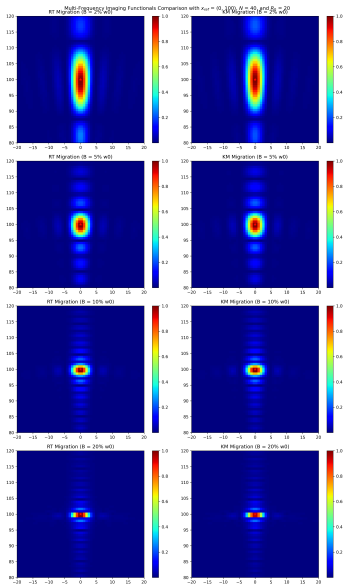
# Time-Dependent (Broadband) – Partial Aperture

**Setup:**  $N = 40$ ,  $R_0 = 20$ , broadband signal  $\hat{f}(\omega) = \mathbf{1}_{[\omega_0-B, \omega_0+B]}(\omega)$ ,  $\omega_0 = 2\pi$ ,  $B = 0.05\omega_0$ ,  $\mathbf{x}_{\text{ref}} = (0, 100)$ .



- The focal spot is significantly more localized than in the monochromatic case: broader frequency content improves coherent focusing.
- Cross-range: RT matches the  $\text{sinc}^2$  main peak and secondary lobes well, confirming the theoretical prediction.
- Range: the profile is consistent with the theoretical  $|\text{sinc}(2B|z - z_{\text{ref}}|)|$  prediction.

# Time-Dependent – Influence of Bandwidth $B$



**Varying bandwidth  $B$ :** wider bandwidth  $\Rightarrow$  sharper range resolution ( $r_I \propto 1/B$ ), cross-range resolution unchanged.

Increasing  $B$  dramatically reduces the range sidelobe level and sharpens the range profile, confirming the sinc dependence on bandwidth.

# Stability – Noisy Model

**Noise model.** The recorded signals are perturbed by complex Gaussian noise:

$$\hat{u}_{rs}^{\text{noisy}}(\omega) = \hat{u}_{rs}(\omega) + W_{rs}^{(1)}(\omega) + i W_{rs}^{(2)}(\omega)$$

where  $W_{rs}^{(1)}, W_{rs}^{(2)} \sim \mathcal{N}(0, \sigma^2/2)$  i.i.d.

## Configurations revisited:

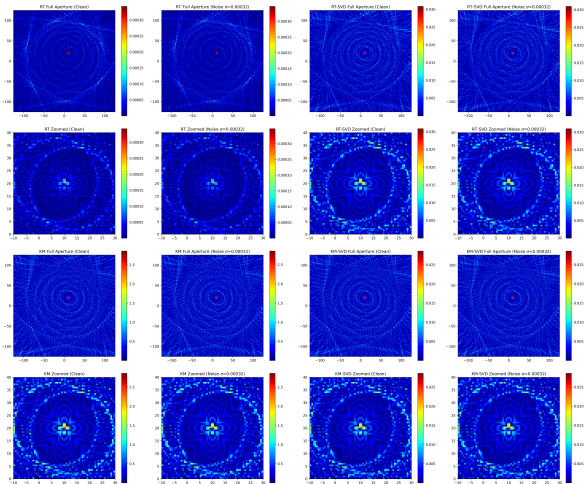
- Full aperture (RT & KM)
- Partial aperture (RT, KM & noise-subspace MUSIC)
- Time-dependent broadband (RT & KM)

**Analysis:** For each configuration, we plot images at increasing  $\sigma$ , then quantify localization error via Monte Carlo simulation (multiple noise realizations).

*Note on MUSIC:* we use the noise-subspace variant

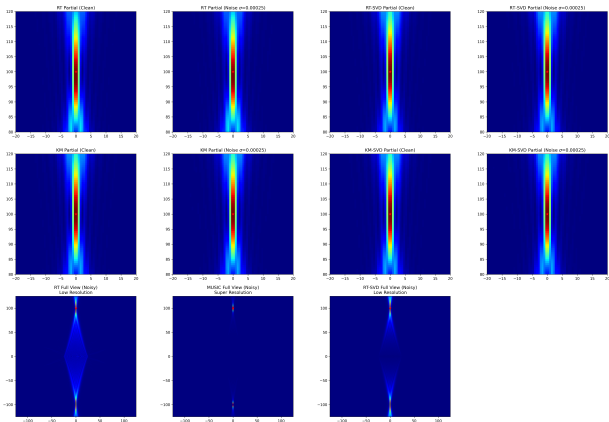
$\mathcal{I}_{MU}(\mathbf{x}) = 1/(1 - |\langle \hat{g}, v_1 \rangle|^2)$  to expose its super-resolution behaviour and its sensitivity to noise.

# Stability – Full Aperture under Noise



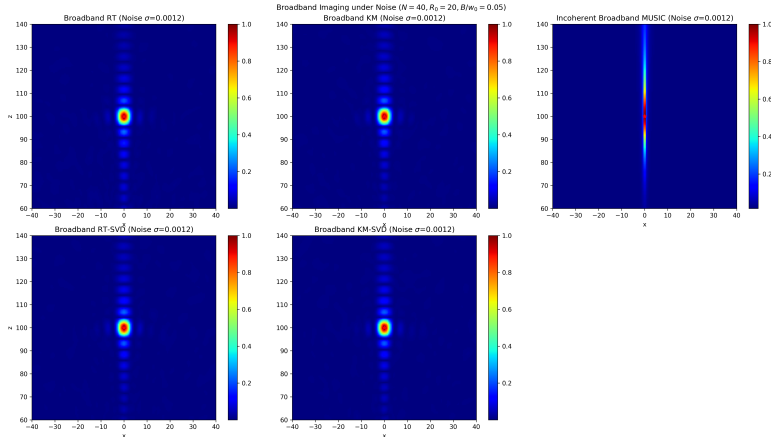
RT and KM both degrade gracefully as  $\sigma$  increases. Coherent integration over many transducer pairs provides a natural averaging effect that partially mitigates noise.

# Stability – Partial Aperture under Noise



RT and KM remain robust for moderate noise levels. The noise-subspace MUSIC functional is sharper at low noise but degrades more abruptly: once the noise level is sufficient to perturb the dominant singular vector  $v_1$ , the localization quality deteriorates rapidly.

# Stability – Time-Dependent Broadband under Noise

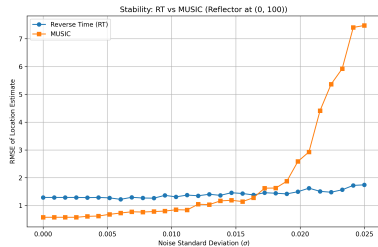


The broadband RT functional retains a well-defined peak even at elevated noise levels, benefiting from frequency diversity in addition to spatial averaging.

# Stability – Monte Carlo Analysis: RT vs. MUSIC

**RMSE of localization vs. noise level  $\sigma$**  (multiple realizations, partial aperture).

- **RT:** localization error grows slowly and steadily with  $\sigma$ . Coherent back-propagation integrates over all source–receiver pairs, averaging out random noise contributions.
- **MUSIC:** error remains very low for small  $\sigma$  (super-resolution), then rises sharply beyond a threshold. Once noise corrupts the dominant singular vector  $v_1$ , the functional fails abruptly.



⇒ RT is more robust; MUSIC offers higher precision at low noise but is fragile.

# Conclusion

## Summary of findings:

- **Full aperture:** RT and KM agree closely; both approach the theoretical  $J_0^2$  focal spot as  $R_0, N \rightarrow \infty$ .
- **Partial aperture:** linear geometry introduces a mirror artifact in range; cross-range resolution scales as  $r_c = \lambda|x_{\text{ref}}|/R_0$ . MUSIC provides a sharper image.
- **Broadband:** increased bandwidth drastically improves range resolution ( $r_l \propto 1/B$ ), consistent with sinc theory.
- **Noise:** RT migration degrades gracefully; MUSIC is precision-first but collapses beyond a noise threshold.

## Perspectives:

- Extension to heterogeneous or anisotropic media.
- Advanced regularization to stabilize MUSIC at high noise.
- Investigation of multiple reflectors and mutual interference.
- Time-reversal approaches in random media.

**Key take-away:** Array geometry, bandwidth and noise level are the three dominant factors controlling resolution and stability of RT/KM imaging functionals.

# Bibliography I

Ammari et al., *Mathematical and Statistical Methods for Multistatic Imaging*, Springer, 2013.